Selection of optimal escape routes in a flood-prone area based on 2D hydrodynamic modelling

Peng Guo, Junqiang Xia, Meirong Zhou, Roger A. Falconer, Qian Chen and Xiaolei Zhang

ABSTRACT

Optimizing escape routes during an extreme flood event is an effective way to mitigate casualties. In this study, a model for selecting optimal escape routes in a flood-prone area has been proposed, which includes a module for predicting the two-dimensional (2D) hydrodynamics and modules for assessing the hazard degree for evacuees, calculation of evacuation times and determination of different escape routes. In the module for determining escape routes, two evacuation schemes were used: scheme A to find optimal escape routes based on established road networks and scheme B to design a new optimal evacuation route. Extreme overbank floods occurred in the Lower Yellow River (LYR) in July 1958 ('58.7') and August 1982 ('82.8') and the proposed model was applied to select the optimal escape routes on a typical floodplain area of the LYR for these two floods. Model predictions indicated that: (i) the optimal escape routes for these two floods were the same for all three starting locations, and the optimized routes provided 3 h more time for evacuees to escape; and (ii) the time of evacuation would need to be earlier for the '58.7' flood because of its larger amount of water volume and higher peak discharge.

Key words | escape route, escape speed, flood-prone area, human stability, hydrodynamic module, Lower Yellow River

Peng Guo
Junqiang Xia (corresponding author)
Meirong Zhou
Qian Chen
Xiaolei Zhang
State Key Laboratory of Water Resources and Hydropower Engineering Science,
Wuhan University,
Wuhan 430072,
China
E-mail: *xiajq@whu.edu.cn*

Roger A. Falconer
Hydro-environmental Research Centre, School of Engineering,
Cardiff University,
Cardiff CF243AA,
UK

INTRODUCTION

As a result of climate change and intensive anthropogenic activities in recent decades, there has been an increasing probability of extreme floods (Milly *et al.* 2002). Various types of floods, such as overbank and urban floods, continue to be regarded as the main sources of casualties for all natural hazards (Niu *et al.* 2013; Xia *et al.* 2014; Zhang *et al.* 2016). According to incomplete statistics, more than 30 overbank flood events have occurred in the Lower Yellow River (LYR) since 1949, with 13,000 villages and 9 million people being affected in total (Niu *et al.* 2013). There is a large inhabitant population living on floodplains, especially in China, which is the world's most populated country (Piao *et al.* 2010). Typically when a farm dyke breaches along a floodplain, rapid flood inundation occurs, resulting in a very limited time for issuing warnings, and the inhabitants usually suffer from potential flood risk (Collier 2007). Therefore, it is desirable to be able to determine optimal escape routes for potential evacuees in terms of flood mitigation for this type of event.

With recent progress in computer-based numerical modelling tools, two-dimensional (2D) hydrodynamic models have been proposed to simulate various processes associated with flood inundation (Liang *et al.* 2007; Neal *et al.* 2009; Xia *et al.* 2010a, 2010b; Liu *et al.* 2015). These model predictions can present temporal and spatial distributions of the key hydrodynamic parameters for a specific flood scenario, such as flow velocity and water depth. As an important tool for current flood-risk management, such model predictions can be used to assess the flood risk to people and provide the potential to instruct local inhabitants

doi: 10.2166/hydro.2018.161

as to when and how to escape in flood-prone areas. Therefore various evacuation algorithms have been developed for people facing extreme flood events. A Life Safety Model (LSM) developed by BC Hydro in Canada offers a robust method for assessing flood risk associated with the operation of dams or other flood control structures (Johnstone *et al.* 2005). As a response planning tool, and a means of calculating complex evacuation processes, an evacuation timeline for flood events is an effective procedure, including: flood inundation extent predictions, warning information delivery, and evacuation operation (Stephen *et al.* 2010). Zhang (2016) analyzed the distribution of water depth in a flood inundation process using the software *MIKE Flood*, and proposed a method to extract impassable flooded roads using *ArcGIS*. Lujak & Giordani (2018) proposed a mathematical model based on two-node centrality measures and the model not only predicts the shortest evacuation route, but also considers other relevant characteristics in order to predict the safest evacuation route. Soon *et al.* (2018) used a semi-parametric estimation method to obtain the marginal effects of explanatory variables on flood victims' evacuation decisions and analyzed the determinants of actual evacuation decisions for an unprecedented 2014 flood disaster. Moshtagh *et al.* (2018) proposed the stochastic queue core (SQC) model for vehicular evacuation problems, with the average travel time and the operation costs being minimized in the model. These models can be integrated, including a module for predicting the flood inundation extent and a module for evacuation planning, to assess the flood risk for the study domain and to provide information for optimal evacuation. However, these models do not consider the stability of victims in floodwaters, and they therefore have limited value in practical decision making for an effective flood evacuation response. Previous studies indicate that the stability degree and escape speed of people in floodwaters can influence the safety and time expenditure for evacuation (Abt *et al.* 1989; Karvonen *et al.* 2000; Ishigaki *et al.* 2008; Xia *et al.* 2014), and these influencing factors need to be considered in the module for selecting optimal escape routes.

Flood risk to people is often estimated empirically according to the magnitude of water depth, which means that the hazard degree of a human body in floodwaters depends solely on the incoming water depth. This method does not account for the effect of flow velocity on the stability of a human body, and therefore does not consider the mechanism of people instability in floodwaters. Various criteria for people instability in floodwaters have been proposed. Abt *et al.* (1989) reported the results of toppling instability experiments of 20 adults, which were conducted in a 61 m-long laboratory flume with different ground surfaces. An equation defining the instability threshold of a person in floodwaters was developed using linear regression of the experimental data. Karvonen *et al.* (2000) undertook stability tests using seven human bodies on a steel grating platform, towed in a model ship basin, and the product of water depth and velocity was proposed to describe the degree of people stability based on their experimental data. Xia *et al.* (2014) derived theoretical formulae for the incipient velocity of a human body in floodwaters for the instability modes of toppling and sliding, with more than 50 tests being undertaken for a model human body, and the experimental data being used to calibrate the parameters in the derived mechanics-based formulae. Furthermore, Ishigaki *et al.* (2008) conducted laboratory experiments on the escape speed for people in floodwaters, with the experimental results indicating that the escape speed is closely related to the water depth. Therefore, the degree of stability and escape speed of people in floodwaters needs to be calculated using hydrodynamic parameters, such as water depth and velocity, and any evacuation prediction method would be more practical and reliable if the instability mechanism of evacuees in floodwaters was included in the analysis.

In this study, a model for selecting optimal escape routes in flood-prone areas is therefore proposed. Two algorithms have been developed to determine optimal escape routes: (i) scheme A – to find the optimal escape routes, based on established road networks, and (ii) scheme B – to design a new optimal evacuation route. The 2D hydrodynamic module was then verified against experimental data for flood flows from two physical models of an idealized city (Soares-Frãzao & Zech 2008) and the Toce River (Soares-Frãzao & Testa 1999). Finally, the proposed model was then applied to select the optimal escape routes for two overbank flood events occurring on the Lankao-Dongming floodplain (LDF) area of the LYR, with the optimal escape routes and corresponding final escape times being determined.

DESCRIPTION OF INTEGRATED MODEL FOR SELECTING OPTIMAL ESCAPE ROUTES

This section gives details of an existing 2D hydrodynamic module, the modules for assessment of the hazard degree for evacuees, the calculation of the evacuation time and determination of different escape routes. In general, these modules are integrated as follows. The temporal and spatial distributions of flood parameters, such as flow velocity and water depth, are initially provided by the 2D hydrodynamic module. Based on these flood parameters, the hazard degree and escape speed of a potential victim, within a computational cell, are then calculated using the calculation modules for the hazard degree and evacuation time of evacuees. Finally, the optimal escape route and corresponding final escape time can be obtained using the module for the determination of different escape routes. Details are given below.

2D hydrodynamic module

In order to simulate the flood inundation processes, the depth-integrated 2D shallow water equations are often used to describe flows in natural rivers, floodplain areas and other flood-prone areas, with the equations being written in a general conservative form as follows (Xia *et al.* 2010a, 2010b):

$$\frac{\partial \boldsymbol{U}}{\partial t}+\frac{\partial \boldsymbol{E}}{\partial x}+\frac{\partial \boldsymbol{G}}{\partial y}=\frac{\partial \tilde{\boldsymbol{E}}}{\partial x}+\frac{\partial \tilde{\boldsymbol{G}}}{\partial y}+\boldsymbol{S} \tag{1}$$

where $\boldsymbol{U}$ = vector of conserved variables; $\boldsymbol{E}$ and $\boldsymbol{G}$ = convective flux vectors for flow in the x and y directions, respectively; $\tilde{\boldsymbol{E}}$ and $\tilde{\boldsymbol{G}}$ = diffusive vectors related to the turbulent stresses in the x and y directions, respectively; and $\boldsymbol{S}$ = source term including bed friction, bed slope and the Coriolis force. The above terms can be written in detail as:

$$\boldsymbol{U}=\begin{bmatrix} h \\ hu \\ hv \end{bmatrix} \boldsymbol{E}=\begin{bmatrix} hu \\ hu^2+\frac{1}{2}gh^2 \\ huv \end{bmatrix} \boldsymbol{G}=\begin{bmatrix} hv \\ huv \\ hv^2+\frac{1}{2}gh^2 \end{bmatrix}$$
$$\tilde{\boldsymbol{E}}=\begin{bmatrix} 0 \\ \tau_{xx} \\ \tau_{yx} \end{bmatrix} \tilde{\boldsymbol{G}}=\begin{bmatrix} 0 \\ \tau_{xy} \\ \tau_{yy} \end{bmatrix} \text{and } \boldsymbol{S}=\begin{bmatrix} 0 \\ gh(S_{bx}-S_{fx}) \\ gh(S_{by}-S_{fy}) \end{bmatrix} \tag{2}$$

where u and v = depth-averaged velocities in the x and y directions, respectively, h = water depth, g = gravitational acceleration, S_{bx} and S_{by} = bed slopes in the x and y directions, respectively, S_{fx} and S_{fy} = friction slopes in the x and y directions, respectively, andτ_{xx} τ_{xy}, τ_{yx} and τ_{yy} = components of the turbulent shear stress over the plane.

A cell-centered finite volume method (FVM) was adopted to solve the governing equations, based on an unstructured triangular mesh. At the interface between two neighboring cells, the calculation of the flow fluxes was treated as a locally one-dimensional problem, thus the flux can be obtained by an approximate Riemann solver. A Roe's approximate Riemann solver, with the scheme of monotone upstream scheme for conservation laws (MUSCL), was employed to evaluate the normal fluxes, and the predictor-corrector procedure was used for time stepping. This approach provided second-order accuracy in both time and space (Tan 1992). The hydrodynamic module was validated using experimental data from two physical models, with the detailed validation process being given in the following section.

Assessment of hazard degree of evacuees

Flood risk to people at various sites varies owing to the difference in flood parameters, and it is important to select an appropriate stability criterion for human subjects in flood risk management. Various criteria have been proposed using theoretical and experimental methods (Abt *et al.* 1989; Karvonen *et al.* 2000; Xia *et al.* 2014). For example, Xia *et al.* (2014) proposed a mechanics-based formula for the incipient velocity of a human body at toppling instability, and accounted for the effect of body buoyancy and the influence of a non-uniform vertical velocity profile acting on the human body in floodwaters, and this formula is given as:

$$U_c=\alpha\left(\frac{h}{h_p}\right)^{\beta}\sqrt{\frac{m_p}{\rho_f h^2}-\left(\frac{a_1}{h_p^2}+\frac{b_1}{hh_p}\right)(a_2 m_p+b_2)} \tag{3}$$

where U_c = incipient velocity of a human body at toppling instability; ρ_f = density of water; h_p and m_p = height and mass of a human body; a_1 and b_1 = non-dimensional coefficients related to the buoyancy force of a human body, with

$a_1 = 0.633$ and $b_1 = 0.367$ for a typical human body of a Chinese person; a_2 and b_2 = coefficients determined from the average attributes of a human body, with $a_2 = 1.015 \times 10^{-3}\ \mathrm{m^3\ kg^{-1}}$ and $b_2 = -4.927 \times 10^{-3}\ \mathrm{m^3}$.

Xia *et al.* (2014) conducted tests in a flume to obtain the water depth and velocity under the condition of toppling instability using a model human body, with the experimental data being used to calibrate two parameters, namely α and β in Equation (3). Figure 1 shows the relationship between the water depth and incipient velocity for a general Chinese adult with a height of 1.71 m and a mass of 68.7 kg, with close agreement being obtained between the calculated and measured data. As shown in Figure 1, the incipient velocity for an adult is $1.3\ \mathrm{m\ s^{-1}}$ for an incoming depth of 0.5 m.

The water depth at a computational cell obtained from the 2D hydrodynamic module is used to calculate the corresponding incipient velocity for a specified adult using Equation (3), as proposed by Xia *et al.* (2014). The following relationship is used to quantify the hazard degree, as given by:

$$HD = Min\ (1.0,\ U/U_c) \tag{4}$$

where HD = hazard degree for a human subject in floodwaters. There are three levels of hazard degree for people in floodwaters according to the value of HD, including: (i) safe ($0 \le \mathrm{HD} < 0.6$), (ii) danger ($0.6 \le HD < 0.9$), and (iii) extreme danger ($0.9 \le HD \le 1.0$) (Cox *et al.* 2010; Xia *et al.* 2014). This mechanics-based assessment method is more practical and reliable because it accounts for the effects of both water depth and flow velocity.

Calculation of evacuation time

There exists a time challenge between people evacuation and flood inundation, because these two processes occur concurrently. Therefore, time is regarded as a key factor in an emergent situation during a flood disaster (Pel *et al.* 2012). The time taken for evacuation is calculated from the escape speed and the corresponding escape distance, which is closely related to the local flow conditions. Ishigaki *et al.* (2008) conducted evacuation tests in a water tank, for water depths varying from 0 to 0.5 m, with and without a flow velocity of $0.5\ \mathrm{m\ s^{-1}}$. A fitted curve based on the measured speeds of escape on foot and the local water depth is shown in Figure 2. The normal walking speeds of people on dry ground are typically 1.35 and $1.27\ \mathrm{m\ s^{-1}}$ for male and female adults, respectively, and the corresponding escape speeds would decrease to 1/2 of the normal walking speed for a typical water depth. However, the transport capacity of a road would also influence the escape speed. An empirical relationship between the water depth and the corresponding escape speed for people is given by:

$$v_E = \begin{cases} \eta \cdot 1.31 - 3.1\,h & (h \le 0.2m) \\ \eta \cdot 0.5\,v_0 & (0.2 \le h \le 0.8m) \end{cases} \tag{5}$$

where v_0 = normal walking speed of adults; v_E = escape speed for people in floodwaters; and η = reduction coefficient of 0.90. Equation (5) shows that it is difficult for people to escape on foot if $h > 0.8$ m.

The flow conditions along an escape route would change with time, and each escape route is then divided into several short segments. For a segment between the locations A_i and A_{i+1} at the time t, a time challenge between people escaping and flood inundation is shown in Figures 3

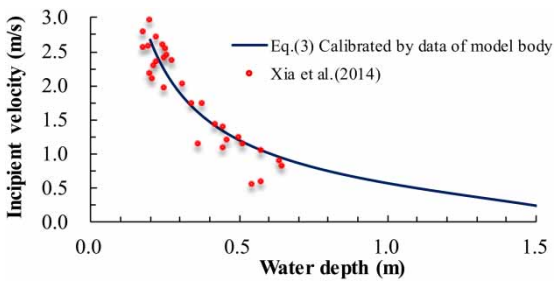

Figure 1 | Instability curves between water depth and incipient velocity for Chinese adults in floodwaters.

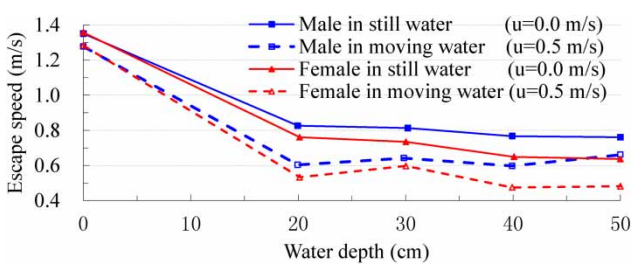

Figure 2 | Empirical curves related to the water depths and corresponding escape speeds for adults in floodwaters (from Ishigaki *et al.* 2008).

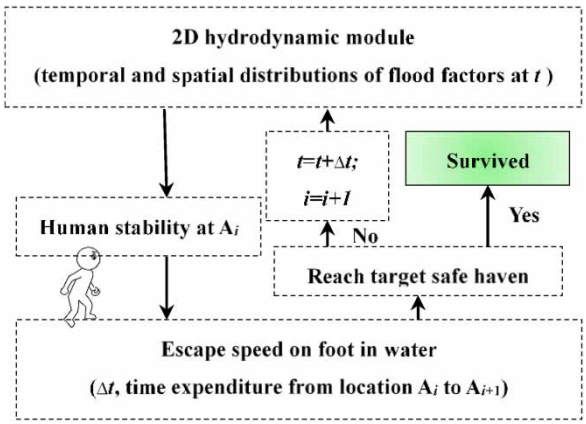

Figure 3 | Time competition between people evacuation and flood inundation.

and 4. The flow conditions at A_i at the time t are determined based on the 2D hydrodynamic module, which can be used to calculate U_c and HD using Equation (3) and Equation (4), respectively. If the value of HD approaches 1.0, namely $U > U_c$, then people in floodwaters would be in danger; otherwise the escape speed of an evacuee can be calculated using Equation (5) and then the time to traverse the segment can be determined. The same approach would be used for the next segment until the location of A_{i+1} is one of the safe havens. The total time of travel along all of the segments from A_1 to A_N is given by:

$$t_N = t_0 + \sum_{i=2}^{N} [\triangle L_{i-1}/(v_{Ei-1})] \quad (6)$$

where t_N = time of travel along the segments from A_1 to A_N; t_0 = initial time for evacuees to receive warning; $\triangle L_{i-1}$ = length of the i–1 segment between the locations A_{i-1} and A_i; and $v_{E,i-1}$ = corresponding escape speed along the i–1 segment.

Determination of different escape routes

In the proposed model, a selection method of optimal escape routes is presented, comprising schemes A and B, under two scenarios i.e. both with and without the established road networks being considered. These two schemes are described in detail as follows.

(1) For a flood-prone area with completed road networks, the Dijkstra algorithm, which can find the shortest path between a given source node and a specified destination node, was adopted to determine the shortest route (Dijkstra 1959). These routes were taken to be alternative escape routes for scheme A. Then the hazard degree for an evacuee, and the corresponding escape speed for each alternative route, were calculated for a specified flood event. When the hazard degree of the route reached 0.9 for the first time, then this time was defined as the final escape time. The route with the latest final escape time was selected as the optimal escape route.

(2) For a flood-prone area with uncompleted road networks, a location was defined as the temporary safe haven if the value of HD for an evacuee is less than 0.6. These locations were zoned by the temporal and spatial distributions of the hydrodynamic parameters for different flood frequency occurrences. For a starting location in the flood-prone area, the corresponding shortest route

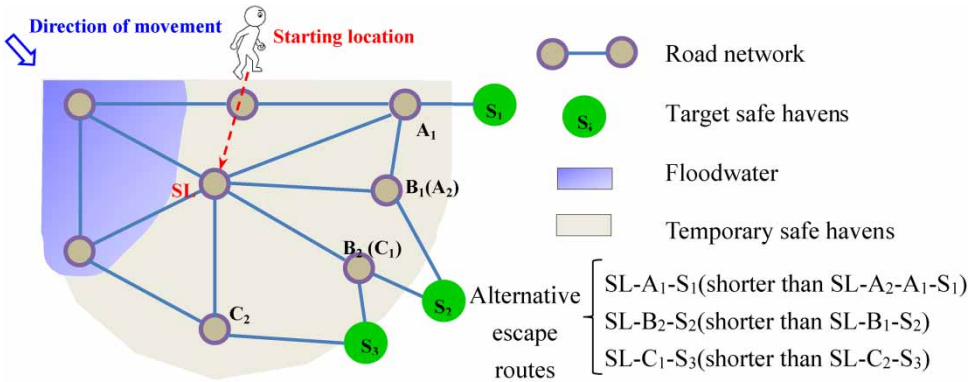

Figure 4 | Sketch diagram for an evacuee to escape in a flood-prone area.

was selected as an optimal escape route to safe havens for scheme B. These routes would provide a reference for the construction of new roads, which would be useful for both transportation and evacuation.

In these two schemes, optimal escape routes and corresponding final escape times can be obtained, which provide a scientific basis for planning evacuation. However, these methods are based more on the mechanics-based stability criterion and escape speed of evacuees, and cannot account for the complicated effects of age, gender and educational level of evacuees.

VERIFICATION OF THE HYDRODYNAMIC MODULE

In order to estimate the escape speed and corresponding flood risk to people, the flood inundation extent is the most important precondition. Therefore, the hydrodynamic module presented above was first verified against experimental data of flood flows based on data from two physical model studies, including: (i) an idealized city (Soares-Frazão & Zech 2008) and (ii) the Toce River (Soares-Frazão & Testa 1999). These results show that the hydrodynamic module can accurately predict various hydrodynamic parameters. The details of the model tests are given in this section.

Flood propagation through an idealized city

Experiments of flood flow through an idealized city were conducted in a 36×3.6 m flume located in the civil engineering laboratory of the Université Catholique de Louvain, Belgium (Soares- Frazão & Zech 2008), with a sketch map of the initial set-up being shown in Figure 5. A gate between the reservoir and downstream was located at $x = 0$ m, and the initial depths were 0.400 m and 0.011 m for the reservoir and downstream, respectively. The sketched city was idealized using 5×5 buildings, which were high enough so that they were not submerged by floodwaters, with the size of each building being 0.3×0.3 m^2 and with the width of each street being 0.1 m.

In the test case, the study domain was divided into 23,346 unstructured triangular cells and the mesh was refined around each building with an area of about 2 cm^2. A free-slip boundary condition was applied at the walls, and a free outflow boundary condition was used at the downstream outlet. A Manning roughness value of 0.010 m$^{-1/3}$ s (Soares-Frazão & Zech 2008), a minimum water depth value of 0.001 m and a time step of 0.0001 s were set to simulate the flood inundation processes occurring after the opening of the gate.

Figure 6 shows the water level profiles along the longitudinal street at $y = 0.2$ m at 5 s and 10 s. It can be seen that the calculated water depth profiles were in close agreement with the measured profiles, with correlation coefficients of $R^2 = 0.88$ and 0.82 at 5 s and 10 s, respectively. However, the calculated depth-averaged velocity profiles were not in such close agreement with the measured data, with correlation coefficients of $R^2 = 0.71$ and 0.75 at the respective times. In most cases the measured water-surface velocities (Soares-Frazão & Zech 2008) were slightly higher than the calculated depth-averaged velocities. This test case therefore indicates that the 2D hydrodynamic module can generally present a credible prediction of the

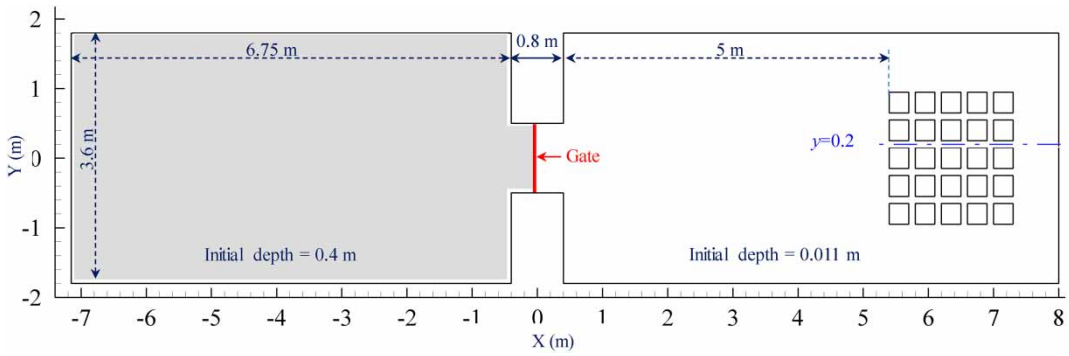

Figure 5 | Sketch of an idealized city in a laboratory flume.

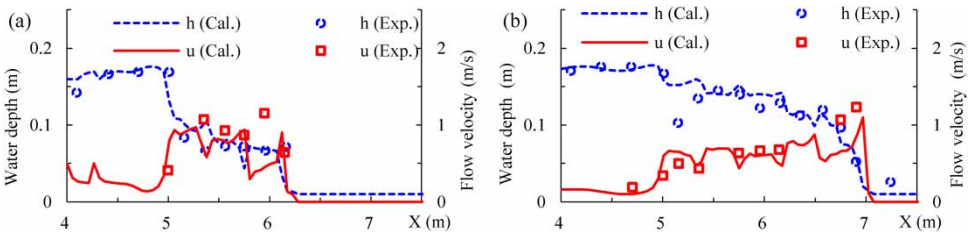

Figure 6 | Comparisons between the calculated and measured water depths and velocities along the longitudinal street at different times of (a) $t = 5$ s and (b) $t = 10$ s.

hydrodynamic parameters for flooding in a scaled model environment.

Flood propagation in the Toce River

A physical model of the Toce River was built at Enel Hydro laboratories in Milan, Italy, consisting of a 1:100 scaled replication of almost 5 km of the river. As shown in Figure 7, a large reservoir was located in the central part of the model, and a set of water probes were located at various monitoring points across the model to record the temporal variation in water level (Soares-Frazão & Testa 1999).

In the test case, the study domain was divided into 21,396 unstructured triangular cells and the mesh was locally refined around the upstream and downstream boundaries and near the reservoir, with the minimum and maximum cell areas being 10 cm^2 and 736 cm^2, respectively. The initial water depth was set to 0.001 m for the dry bed of the domain and a free outflow boundary condition was applied at the downstream outlet. A constant time step of $\Delta t = 0.001$ s and a constant Manning's roughness coefficient of $n = 0.0162\ m^{-1/3}s$ (Soares-Frazão & Testa 1999) were adopted in the module. In addition, the minimum water depth for treating the wetting and drying fronts was set to 0.001 m for this study.

Figure 8 shows the variation in the measured and calculated water levels at the sites of P_1, P_4, P_{13} and P_{19}. It can be seen that the calculated depths were in close agreement with the measured values, with correlation coefficients of $R^2 =$ 0.84, 0.75, 0.70 and 0.88, respectively. It was concluded from these comparisons that the 2D hydrodynamic module was accurately predicting the hydrodynamic parameters in a flood-prone area with complex topography.

MODEL APPLICATION

Study area

In order to determine optimal escape routes in the LDF, related measurements were collected from the YRCC (Yellow River Conservancy Committee), including: topography, surface landforms, overbank floods occurring in the Dongming floodplain area, and discharge hydrographs at Jiahetan for the years 1958 and 1982. In total there are about 120 natural floodplain areas in the LYR, which are inhabited by 1.9 million residents, with overbank flood events frequently occurring on the LDF area during flood seasons. In particular, there was also a serious flood on the LDF area in 2003 due to a farm-dyke breach, with 114

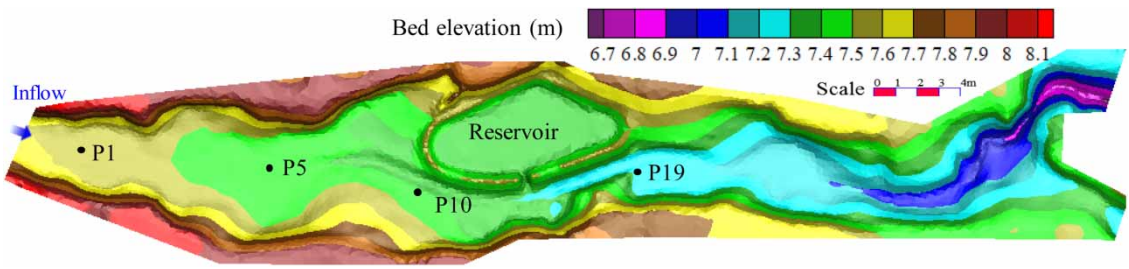

Figure 7 | Topography of the Toce River physical model showing the locations of monitoring points.

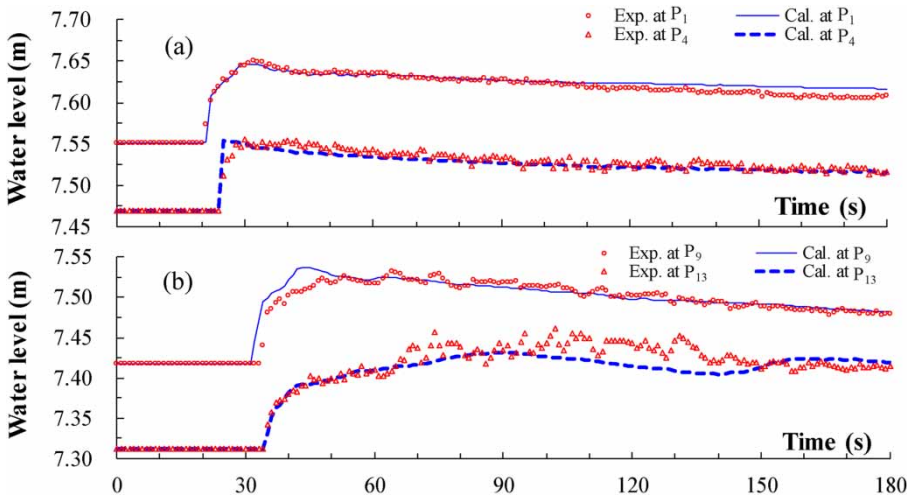

Figure 8 | Comparisons between the calculated and measured water levels at different monitoring points of (a) P_1 and P_4; and (b) P_9 and P_{13}.

villages and 12,000 hm^2 of farmland being submerged, and with 160,000 people being affected. Therefore, it is important for people living on flood-prone areas to be able to escape efficiently in emergency situations. Two extreme overbank floods occurred on the LDF area in July 1958 and August 1982, with the corresponding peak discharges being 20,500 and 14,500 $m^3 s^{-1}$, respectively, at the hydrometric station of Jiahetan (Figure 9). The proposed model was applied to select optimal escape routes for these two overbank flood events, assuming that the discharge hydrograph entering the floodplain zone for each flood scenario was equivalent to the hydrograph at Jiahetan, minus the current bankfull discharge (7,000 $m^3 s^{-1}$) along this reach. The locations of a flood diversion sluice, three starting locations ($SL_{1\text{-}3}$), two observation points (P_1 and P_2) and target safety areas are shown in Figure 9. The flood inundation extent on the LDF area during the '82.8' flood are given in detail. Comparisons of the locations and final escape times for optimal escape routes are presented for the '58.7' and '82.8' flood events.

Simulation of '82.8' overbank flood

The study domain covered an area of about 250 km^2 and was divided into 16,064 unstructured triangular cells, which included a significant slope in the southeast direction of the LDF area (Figure 10). The simulation conditions included: a constant time step of 0.2 s, and a constant Manning roughness coefficient of 0.060 $m^{-1/3}s$ for village areas and 0.035 $m^{-1/3}s$ for other underlying surfaces (Zhang *et al.* 2016).

As shown in Figure 11, the corresponding water depth was 1.2 m when the hazard degree for people at P_1 reached 1.0 at $t = 10.9$ h; however, the corresponding water depth was 1.4 m when the hazard degree for people at P_2 was equal to 1.0 at $t = 35.6$ h. The location of P_1 was near the flood diversion sluice, with the local velocity being higher than that at P_2. Thus, it is more reliable to evaluate human stability using Equations (3) and (4), because people would be swept away under the condition of small water depth and large flow velocity.

In addition, the hazard degree distributions for people at $t = 9$, 13 and 33 h are shown in Figure 12. It can be seen that the area including the dangerous zone would increase gradually along the levee due to the relatively large slope in the southeast direction on the LDF area. All the inhabitants would be in danger at $t = 49$ h, and they would have to escape according to the optimal route.

Determination of optimal escape routes in the '82.8' overbank flood

Optimal escape routes for scheme A

The optimal escape routes for scheme A are presented for three starting locations. As shown in Figure 9, five alternative routes for each starting location are presented using the

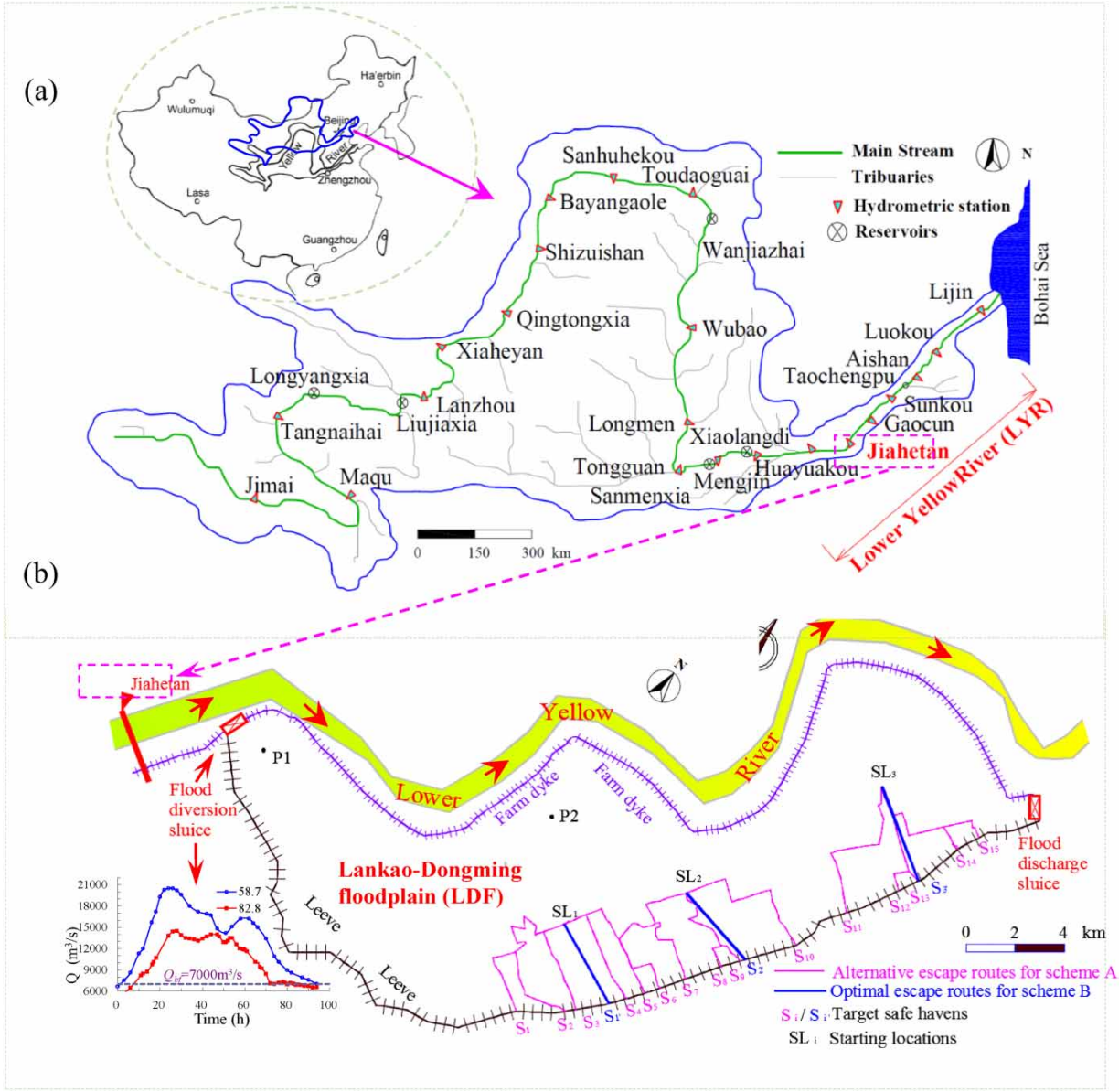

Figure 9 | (a) Sketch of the Lower Yellow River. (b) Alternative escape routes for scheme A and optimal escape routes for scheme B for the Lankao-Dongming floodplain area.

Dijkstra algorithm, with the optimal escape routes for scheme A being selected. The variation in the hazard degree for evacuees along the optimal routes and the worst routes for the three starting locations are shown in Figure 13. The duration was only about 1.5 h when the *HD* value increased from 0.0 to 1.0 for each escape route. However, the evacuees at SL_1 would eventually be rescued if they selected the worst route S_1 to escape and were aware of the danger before $t = 5.9$ h, as the *HD* value was equal to 0.9. Similarly, they would eventually be rescued if they were aware of the danger and selected the optimal route S_5 to escape before $t = 10.7$ h. Therefore, the route S_5 was selected as the optimal route for SL_1, with the corresponding final escape time being $t = 10.7$ h. In a similar manner, the route S_9 was selected as the optimal route for SL_2, with the corresponding final escape time of $t = 11.7$ h; and the route S_{13} was selected as the optimal route for SL_3, with the corresponding final escape time being $t = 14.7$ h.

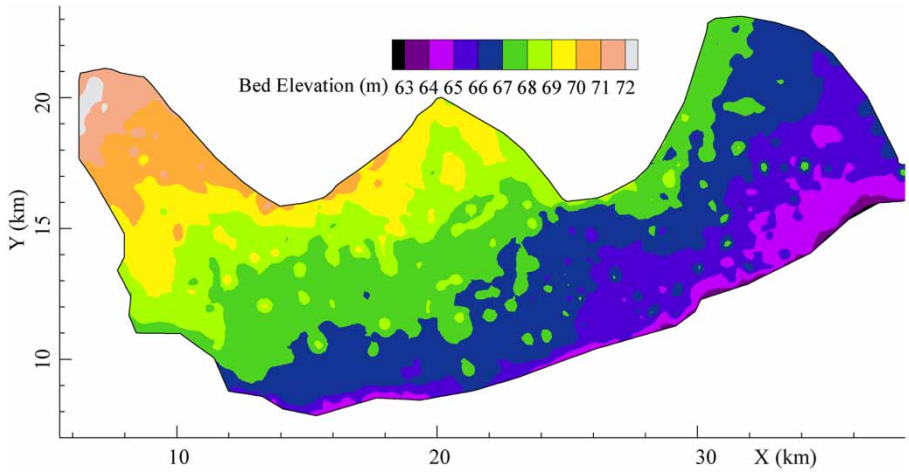

Figure 10 | Topography of the study domain.

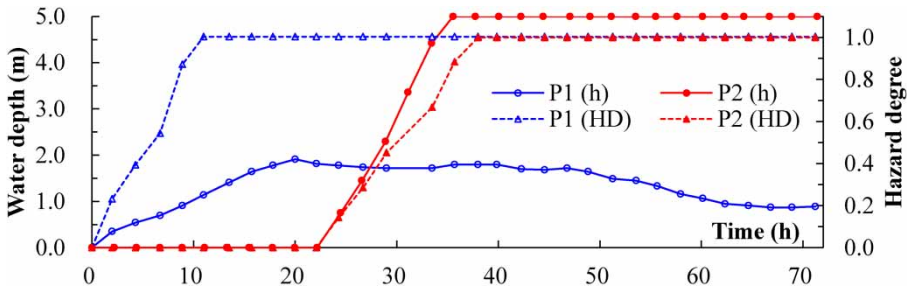

Figure 11 | Temporal variations in water depth and hazard degree for people at different points of P1 and P2.

Optimal escape routes for scheme B

People need to escape at SL_1, SL_2 and SL_3 since they would be in danger if they were not aware of warnings before $t = 19.9$, 20.7 and 22.2 h. The optimal escape routes for scheme B are presented in Figure 9, with the corresponding final escape times being given in Table 1. For example, the period from the time when people started to escape at $t =$ 19.9 h increased gradually, and the temporary safe haven would border on the target safe haven at S_1 for the first time after a period of 6.7 h. Thus, the final escape time would be $t = 13.2$ h if evacuees chose the route $SL_1 \sim S_1$. In a similar way, the final escape times were $t = 16.6$ h and 17.5 h if evacuees selected the routes $SL_2 \sim S_2$ and $SL_3 \sim S_3$, respectively.

A comparison of the final escape times between schemes A and B is shown in Table 1. Compared with the optimal routes for scheme B, the time for inhabitants to evacuate based on the optimal times for scheme A were 2.5, 4.9 and 2.8 h, respectively, for the three routes considered. The optimal route $SL_2 \sim S_2$ was close to the route $SL_2 \sim S_9$, and the optimal route $SL_3 \sim S_3$ was also close to $SL_3 \sim S_{13}$. The results provide evidence for adjusting the existing routes slightly. However, the optimal route $SL_1 \sim S_1$, was very different from the route $SL_1 \sim S_5$. Thus, for a flood-prone area with an incomplete road network, the construction of new routes can be considered based on the current calculation results, since the routes would be useful for evacuation and transportation.

Optimal escape routes for the '58.7' overbank flood event

The optimal escape routes and corresponding final escape times were also calculated for the '58.7' overbank flood event, with the results for schemes A and B being shown

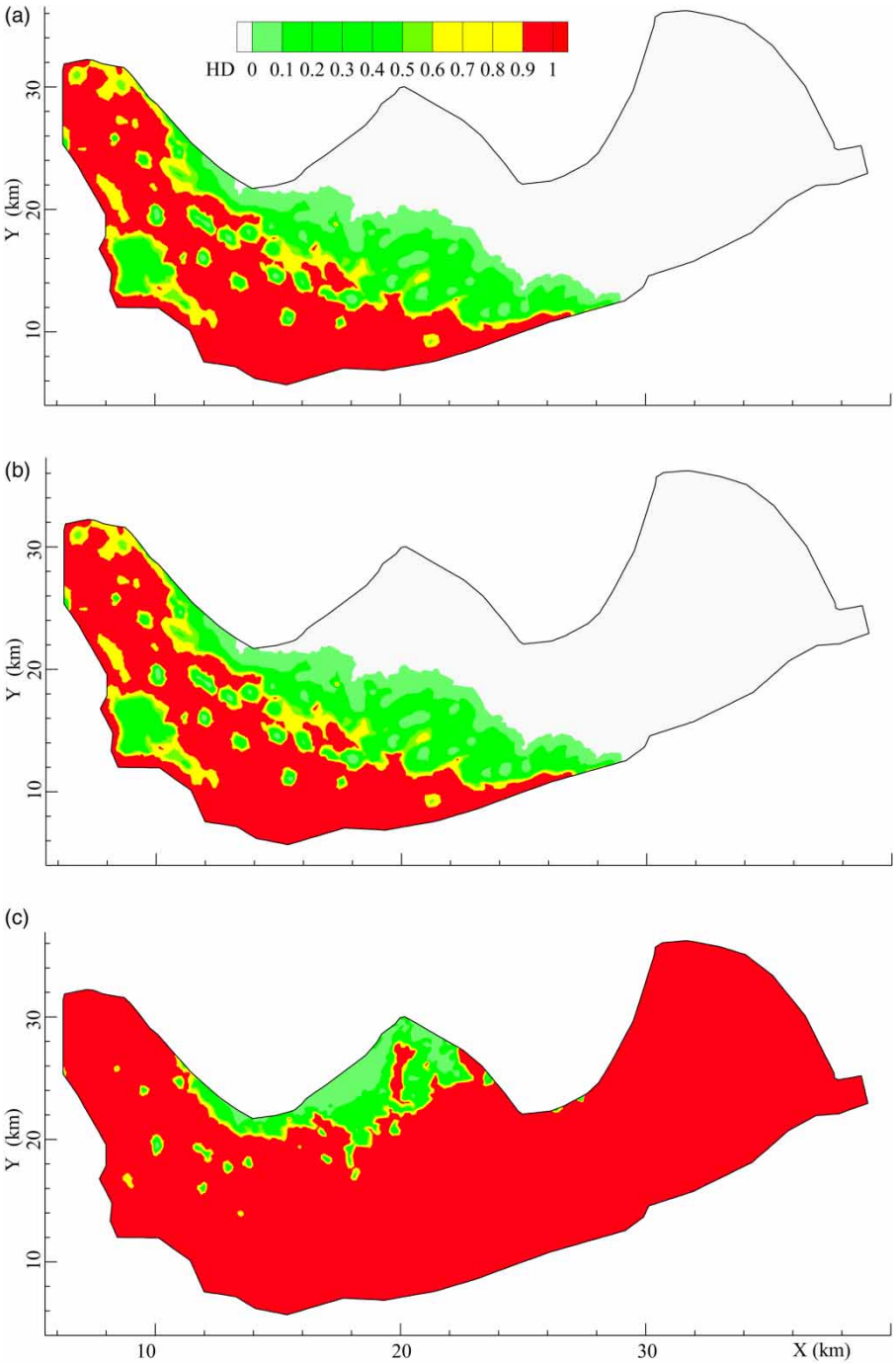

Figure 12 | Distributions of hazard degree for people at different times of (a) t = 9 h, (b) t = 13 h and (c) t = 33 h.

in Table 1. The optimal escape routes were the same for these two overbank floods, for both schemes A and B, but the corresponding final escape times for scheme A for the '58.7' flood event were 1–3 h earlier than those for the '82.8' flood event, and the final escape times for scheme B for the '58.7' flood event were about 3 h earlier than those for the '82.8' flood event. A comparison of these results indicates that the optimal escape routes for the three starting

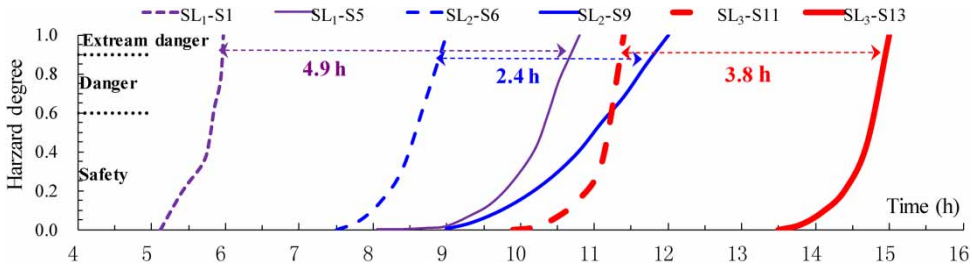

Figure 13 | Temporal variations in hazard degree for people using alternative routes.

Table 1 | Optimal escape routes and corresponding final escape times for the '58.7' and '82.8' overbank flood events

Floods		Scheme A			Scheme B		
'82.8'	Optimal escape routes	$SL_1 \sim S_5$	$SL_2 \sim S_9$	$SL_3 \sim S_{13}$	$SL_1 \sim S_{1'}$	$SL_2 \sim S_{2'}$	$SL_3 \sim S_{3'}$
	Final escape moments (h)	10.7	11.7	14.7	13.2	16.6	17.5
'58.7'	Optimal escape routes	$SL_1 \sim S_5$	$SL_2 \sim S_9$	$SL_3 \sim S_{13}$	$SL_1 \sim S_{1'}$	$SL_2 \sim S_{2'}$	$SL_3 \sim S_{3'}$
	Final escape moments (h)	8.4	10.2	13.2	10.5	13.4	14.9

locations could be determined, but the corresponding final escape times for the '58.7' flood event were earlier since the peak discharge and water volume for the '58.7' flood event were greater than those for the '82.8' flood event. These results mean that the escape routes would be the same for floods with different occurrence frequencies, but the final escape times should be calculated based on the model predictions of flood inundation processes.

CONCLUSIONS

In the current study, an integrated numerical model has been developed to select optimal escape routes in flood-prone areas, with the model including a module for predicting the 2D hydrodynamics, and additional modules for assessing the hazard degree for evacuees, the calculation of evacuation times and the determination of different escape routes. The conclusions obtained from this study can be summarized as follows.

A 2D hydrodynamic module was used to simulate the flood inundation extent and processes over a flood-prone area. A detailed validation process was undertaken of the model, which showed that the hydrodynamic module was capable of predicting the hydrodynamic parameters over complex urban and rural topographies. The mechanics-based formula for the incipient velocity of a human body at toppling instability was adopted to assess the stability degree of evacuees in floodwaters. An empirical relationship between the water depth and corresponding escape speed was used to calculate the cumulative time required for evacuation. The selection method of optimal escape routes was presented, comprising schemes A and B, and for scenarios with and without established road networks being considered.

Model application in the LDF area showed that optimal escape routes and corresponding final escape times were determined for three starting locations, for schemes A and B, for the '58.7' overbank flood event, which would provide about another 3 h and 5 h for issuing warnings and evacuation procedures compared with the worst escape routes. The optimal escape routes for the '82.8' and '58.7' overbank flood events were the same as for the previous three starting locations. However, the final escape time for the '58.7' overbank flood event would be earlier since there was a larger water volume and a higher peak discharge.

ACKNOWLEDGEMENTS

The study was partly supported by the National Natural Science Foundation of China (Grant Nos. 51725902 and

51579186) and the Key Cultivating Project from Wuhan University (Grant No. 2042017kf0238). It was also partly supported by two international projects of the Global Challenges Research Fund at Cardiff University and the UK-China Urban Flooding Research Impact Programme.

REFERENCES

Abt, S. R., Wittler, R. J., Taylor, A. & Love, D. J. 1989 Human stability in a high flood hazard. *Water Resources Bulletin* **25**, 881–890.

Collier, C. G. 2007 Flash flood forecasting: what are the limits of predictability? *Quarterly Journal of the Royal Meteorological Society* **133**, 3–23.

Cox, R. J., Shand, T. D. & Blacka, M. J. 2010 *Australian Rainfall and Runoff: Appropriate Safety Criteria for People*. Report P10/S1/006. Engineers Australia, Barton, ACT, Australia.

Dijkstra, E. W. 1959 A note on two problems in connexion with graphs. *Numerische Mathematik* **1**, 269–271.

Ishigaki, T., Kawanaka, R., Onishi, Y., Shimada, H., Toda, K. & Baba, Y. 2008 Assessment of safety on evacuating route during underground flooding. In: *Proceedings of 16th IAHR-APD Congress and 3rd Symposium of IAHR-ISHS*, Nanjing, China, pp. 141–146.

Johnstone, W. M., Sakamoto, D., Assaf, H. & Bourban, S. 2005 Architecture, Modelling Framework and Validation of BC Hydro's Virtual Reality Life Safety Model. In: *International Symposium on Stochastic Hydraulics*, Nijmegen, The Netherlands, pp. 23–24.

Karvonen, R. A., Hepojoki, H. K., Huhta, H. K. & Louhio, A. 2000 *The Use of Physical Models in Dam-Break Analysis*. RESCDAM Final Report. Helsinki University of Technology, Helsinki, Finland, p. 57.

Liang, D. F., Lin, B. L. & Falconer, R. A. 2007 A boundary-fitted numerical model for flood routing with shock-capturing capability. *Journal of Hydrology* **332**, 477–486.

Liu, Q., Qin, Y., Zhang, Y. & Li, Z. W. 2015 A coupled 1D-2D hydrodynamic model for flood simulation in flood detention basin. *Natural Hazards* **75**, 1303–1325.

Lujak, M. & Giordani, S. 2018 Centrality measures for evacuation: finding agile evacuation routes. *Future Generation Computer Systems* **83**, 401–412.

Milly, P. C. D., Wetherald, R. T., Dunne, K. A. & Delworth, T. L. 2002 Increasing risk of great foods in a changing climate. *Nature* **415**, 514–517.

Moshtagh, M., Fathali, J. & Smith, M. J. 2018 The Stochastic Queue Core problem, evacuation networks, and state-dependent queues. *European Journal of Operational Research* **269**, 730–748.

Neal, J., Fewtrell, T. & Trigg, M. 2009 Parallelisation of storage cell flood models using OpenMP. *Environmental Modelling and Software* **24**, 872–877.

Niu, Y. G., Danmu, L. M., Geng, M. Q. & Li, Y. Q. 2013 Discussion on zoned harnessing of the lower Yellow River floodplain. *Yellow River* **35**, 7–9. 13 (in Chinese).

Piao, S. L., Ciais, P., Huang, Y., Shen, Z. H., Peng, S. S., Li, J. S., Zhou, L. P., Liu, H. Y., Ma, Y. C., Ding, Y. H., Friedlingstein, P., Liu, C. Z., Tan, K., Yu, Y. Q., Zhang, T. Y. & Fang, J. Y. 2010 The impacts of climate change on water resources and agriculture in China. *Nature* **467**, 43–51.

Pel, A. J., Bliemer, M. C. & Hoogendoorn, S. P. 2012 A review on travel behavior modelling in dynamic traffic simulation models for evacuations. *Transportation* **39**, 97–123.

Soares-Frazão, S. & Testa, G. 1999 The Toce River test case: Numerical results analysis. In: *Proceedings of 3rd CADAM Meeting, 6th–7th May*, Milan, Italy, p. 10.

Soares-Frazão, S. & Zech, Y. 2008 Dam-Break flow through an idealized city. *Journal of Hydraulic Research* **46**, 648–658.

Soon, J. J., Kamaruddin, R. & Anuar, A. R. 2018 Flood victims' evacuation decisions: a semi-nonparametric estimation. *International Journal of Emergency Services* **7**, 134–146.

Stephen, O., Peter, C. O. & Belinda, D. 2010 Timeline modelling of flood evacuation operations. *Procedia Engineering* **3**, 175–187.

Tan, W. Y. 1992 *Shallow Water Hydrodynamics: Mathematical Theory and Numerical Solution for A Two-Dimensional System of Shallow Water Equations*. Elsevier, New York.

Xia, J. Q., Falconer, R. A., Wang, Y. J. & Xiao, X. W. 2014 New criterion for the stability of a human body in floodwater. *Journal of Hydraulic Research* **53**, 93–104.

Xia, J. Q., Falconer, R. A., Lin, B. L. & Tan, G. M. 2010a Modelling dam-break flows over mobile beds using a 2D coupled approach. *Advances in Water Resources* **33**, 171–183.

Xia, J. Q., Falconer, R. A., Lin, B. L. & Tan, G. M. 2010b Modelling floods routing on initially dry beds with the refined treatment of wetting and drying. *International Journal of River Basin Management* **8**, 225–243.

Zhang, W. 2016 Emergency evacuation planning against dike-break flood a GIS-based DSS for flood detention basin of Jingjiang in central China. *Natural Hazards* **81**, 1283–1301.

Zhang, X. L., Xia, J. Q. & Li, N. 2016 Impacts of mesh scale and village region roughness on predictions of flood inundation over complex floodplains. *Journal of Hydroelectric Engineering* **35**, 48–57 (in Chinese).

First received 3 December 2017; accepted in revised form 23 July 2018. Available online 7 September 2018